International Journal of Engineering Inventions
e-ISSN: 2278-7461, p-ISSN: 2319-6491
Volume 15, Issue 8 [August 2026] PP: 32-39

Robust Fuzzy-PID Speed Regulation of an Isolated Hydropower Plant Integrated with Photovoltaic and Wind Generation

Duy-Trung Nguyen[1,*], Mai-Duyen Nguyen-Thi[1], Huy-Hoang Hoang[1], Huy-Tan Pham-Nhat[1], Thu-Ha Nguyen[2], Ba-Kha Nguyen[2]
[1]*Faculty of Control and Automation, Electric Power University, Hanoi, Vietnam*
[2]*School of Electrical and Electronic Engineering (SEEE), Hanoi University of Industry, Hanoi, Vietnam*
[*]*Corresponding Author: trungnd@epu.edu.vn*

ABSTRACT: *This paper develops a transparent fuzzy-logic gain-scheduled PID controller for generator-speed regulation in an isolated hydro-photovoltaic-wind grid. The model retains water-column and gate-servomotor dynamics, aggregate inertia, load damping, renewable-power intermittency, gate saturation, and gate-rate limitation. Proportional, integral, and derivative gains are scheduled from normalized frequency error and error rate through explicit Takagi-Sugeno surfaces. PI, fixed PID, fuzzy-PI, and fuzzy-PID are tested under three 200 s scenarios: mixed load/renewable variation, a severe combined power deficit, and persistent multi-sine disturbances. Performance is evaluated by peak and RMS error, IAE, ISE, ITAE, ITSE, and RMS gate movement. In Scenario 1, fuzzy-PID limits the peak deviation to 0.1307 Hz and reduces IAE by 20.7% relative to fixed PID. Under the severe test, its IAE is 15.407 Hz·s, compared with 18.775 Hz·s for PID and 17.412 Hz·s for fuzzy-PI. Forty Monte-Carlo realizations with independent ±20% variations in inertia, damping, governor time, and water starting time preserve the same ordering; the fuzzy-PID median IAE is 15.369 Hz·s. No unstable realization is observed. The gain schedule improves frequency quality without a material rise in RMS gate motion, providing a reproducible simulation baseline for hydro-led isolated grids.*

Keywords: *fuzzy logic control; hydropower governor; isolated grid; load-frequency control; photovoltaic generation; renewable integration; speed regulation; wind power.*

Date of Submission: 11-08-2026 Date of acceptance: 24-08-2026

I. INTRODUCTION

Isolated grids have little or no external frequency support. Their instantaneous power imbalance must therefore be absorbed by locally available inertia and controllable generation. Photovoltaic (PV) and variable-speed wind converters reduce fuel consumption and operating emissions, but their weather-dependent active power and limited natural inertial response increase the burden on the synchronous hydropower unit [1]-[5]. The broader automatic-generation-control context is synthesized in [2]. Hydropower is well suited to this role because it can sustain regulation; nevertheless, water starting time, inverse hydraulic response, gate dead zones, and generation-rate limits make aggressive tuning unsafe [6]-[8]. Experimental work on variable-speed hydropower further confirms that the plant model and control law must be assessed together [7].

Conventional PI and PID governors remain attractive because they are transparent and easy to commission. Their fixed gains, however, represent one compromise between small-signal recovery and large-disturbance damping. Fuzzy gain scheduling has consequently been applied to load-frequency control, renewable microgrids, and hydrothermal systems [9]-[15]. Recent work includes fuzzy adaptive predictive control for isolated microgrids [10], optimal fuzzy PIDF control [12], ultra-local fuzzy PIDF control [13], and higher-order or type-3 fuzzy schemes [14], [15]. These studies demonstrate the potential of intelligent scheduling, but comparisons sometimes change the actuator model or retune each controller separately, obscuring whether the improvement comes from the control law or the test protocol.

This study provides a compact and reproducible hydro-led benchmark. The contributions are: (i) an isolated hydro-PV-wind model with identical gate magnitude and rate constraints for all controllers; (ii) a two-input fuzzy scheduler that modifies all three PID gains through an explicit analytical rule surface, avoiding an opaque optimizer; (iii) three distinct disturbance scenarios and comparison against PI, fixed PID, and fuzzy-PI using IAE, ISE, ITAE, and ITSE; and (iv) a forty-run ±20% uncertainty assessment using MATLAB software. The aim is not to claim field validation, but to provide a technically auditable simulation study and a defensible path toward hardware-in-the-loop testing.

II. HYBRID ISOLATED-GRID MODEL

A. Power balance and frequency dynamics

The hydro generator is the grid-forming source, whereas PV and wind plants operate as grid-following active-power injections around their scheduled operating points. With incremental quantities expressed in per unit, the aggregate swing equation is

$$2H \frac{d(\Delta f)}{dt} = \Delta P_H + \Delta P_{PV} + \Delta P_W - \Delta P_L - D\Delta f \quad (1)$$

where H is the equivalent inertia constant, D is the load-frequency coefficient, and ΔP_H, ΔP_{PV}, ΔP_W, and ΔP_L denote hydro, PV, wind, and load-power deviations. The nominal frequency is 50 Hz. This reduced-order model is appropriate for controller-level frequency studies; converter inner loops are assumed faster than hydro-governor dynamics [3], [4], [16].

B. Governor and hydraulic turbine

The gate servomotor is represented by a first-order state with explicit magnitude and rate limits:

$$\frac{d(\Delta g)}{dt} = sat_{\pm G_r}\{\frac{sat_{\pm G\square}(u) - \Delta g}{T_g}\} \quad (2)$$

For the non-elastic water column, the incremental water-flow state is

$$\frac{d(\Delta q)}{dt} = \frac{\Delta g - \Delta q}{T_w}, \quad \Delta P_H = \Delta q \quad (3)$$

The simplified realization preserves the dominant gate-to-power delay while allowing every simulation and uncertainty realization to be reproduced without proprietary component libraries. The limits are G□ = 0.16 pu and G_r = 0.12 pu/s. Figure 1 shows the information and power flow.

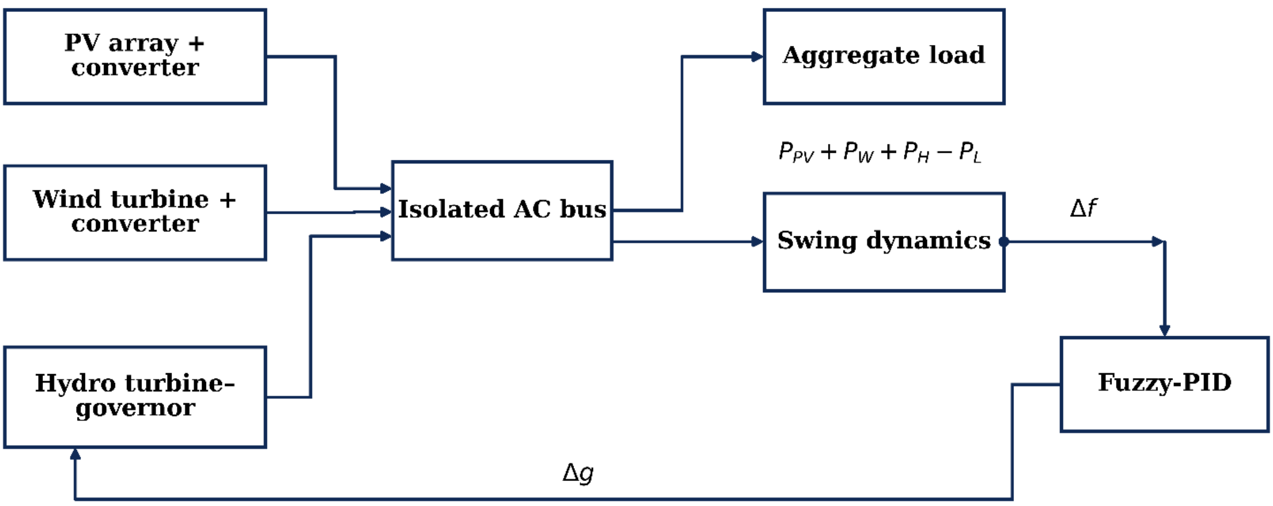

Fig. 1. Hydro-PV-wind isolated-grid model and fuzzy-PID feedback path.

Table 1. Nominal model and simulation parameters.

Quantity	Symbol	Value	Quantity	Symbol	Value
Nominal frequency	f_0	50 Hz	Inertia constant	H	4.6 s
Load damping	D	1.05 pu/pu	Governor time	T_g	0.32 s
Water time	T_w	1.65 s	Gate limit	G_m	±0.16 pu
Gate-rate limit	G_r	±0.12 pu/s	Step size	Δt	0.05 s
Simulation horizon	T_f	200 s	Uncertainty	—	±20%

III. CONTROL DESIGN

A. Baseline PI and PID controllers

Let e = −Δf be the secondary frequency error. The common filtered PID form is

$$u = K_p e + K_i \int e\, dt + K_d \left[\frac{N}{s+N}\right] \frac{de}{dt} \quad (4)$$

Anti-windup is activated when the command reaches its saturation bound. The comparison uses PI gains (Kp, Ki) = (1.10, 0.42) and PID gains (Kp, Ki, Kd) = (1.45, 0.58, 0.10). These gains were selected on the nominal model and then held fixed for all tests.

B. Proposed fuzzy-PID gain scheduler

The fuzzy scheduler uses the normalized error magnitudes a and b, limited to the unit interval:

$$a = min(1, \frac{|e|}{e_s}), \quad b = min(1, \frac{|\dot{e}|}{\dot{e}_s}) \quad (5)$$

with $e_s = 0.0035$ pu and $\dot{e}_s = 0.010$ pu/s. The triangular linguistic partitions Small, Medium, and Large lead to a smooth singleton surface. Its closed-form implementation is

$$K_{p*} = K_p(1 + 0.62a + 0.18b) \quad (6)$$

$$K_{i*} = K_i(1 + 0.35a)(1 - 0.42b) \quad (7)$$

$$K_{d*} = K_d(1 + 0.75b) \quad (8)$$

Equations (6)-(8) are equivalent to a nine-rule Takagi-Sugeno scheduler with weighted-average defuzzification. Large frequency error strengthens proportional action; a fast error trajectory increases derivative damping and temporarily reduces integral action; near equilibrium, integral authority returns to remove steady-state offset. This structure is interpretable and avoids dependence on a metaheuristic optimum whose repeatability may be sensitive to initialization [11]-[15].

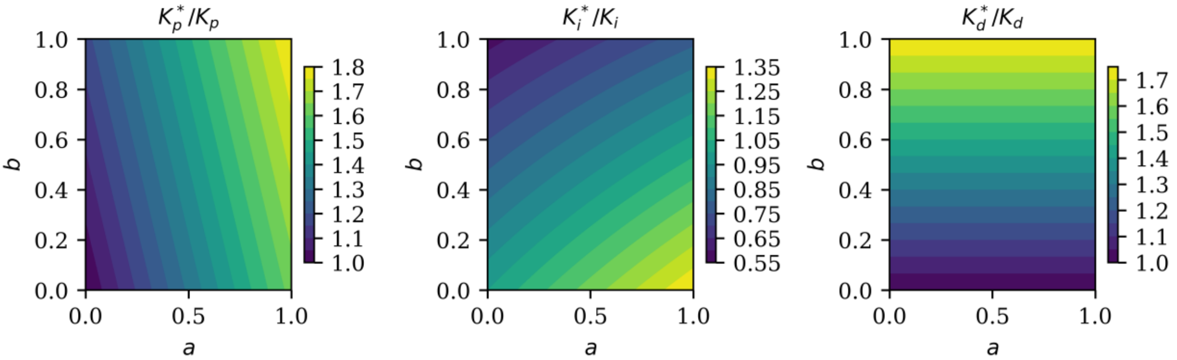

Fig. 2. Normalized fuzzy gain surfaces used for online PID scheduling.

Figure 2 makes the scheduling mechanism explicit. The proportional surface rises with both error magnitude and error rate. The integral surface behaves differently: it recovers near steady state but is suppressed during a fast transient. Derivative action is governed mainly by the normalized error rate. This separation is deliberate. It limits integral accumulation without sacrificing damping.

Table 2. Controllers compared under identical constraints.

Controller	Kp	Ki	Kd	Online scheduling
PI	1.10	0.42	0	No
PID	1.45	0.58	0.10	No
Fuzzy-PI	1.25	0.52	0	Kp, Ki
Proposed fuzzy-PID	1.50	0.62	0.12	Kp, Ki, Kd

IV. SIMULATION PROTOCOL

Three 200 s scenarios are considered. Scenario 1 combines four load steps, two PV cloud-edge ramps, and multisine wind variation. Scenario 2 is deliberately severe: a larger load increase is followed by an extended PV deficit, a temporary load pulse, and a delayed wind-power reduction. Scenario 3 uses persistent multisine variations plus a short cloud event. The initial dispatch is balanced at PL = 0.42 pu, PPV = 0.16 pu, PW = 0.13 pu, and PH = 0.13 pu. Every controller receives identical disturbances and obeys the same gate-position and gate-rate limits. No gain is retuned between scenarios.

The midpoint Runge-Kutta integration step is 0.05 s. Performance is evaluated through peak and RMS frequency deviation, RMS gate movement, and four integral criteria. IAE and ITAE are defined by

$$J_{IAE} = \int_0^{T_f} |\Delta f(t)|\, dt, \quad J_{ITAE} = \int_0^{T_f} t|\Delta f(t)|\, dt \quad (9)$$

$$g_{rms} = \sqrt{\frac{1}{T_f}\int_0^{T_f} [\Delta g(t)]^2\, dt} \quad (10)$$

ISE and ITSE use the same limits with $|\Delta f|$ replaced by $(\Delta f)^2$ and $t|\Delta f|$ replaced by $t(\Delta f)^2$, respectively. These four indices distinguish amplitude suppression from late-error suppression. Robustness is then evaluated using forty seeded realizations. H, D, Tg, and Tw vary independently within ±20%; the severe Scenario 2 is repeated without controller retuning. The all-in-one m-file regenerates the profiles, integration, figures, tables, and Monte-Carlo sample.

V. RESULTS AND DISCUSSION

A. Mixed step and renewable variations

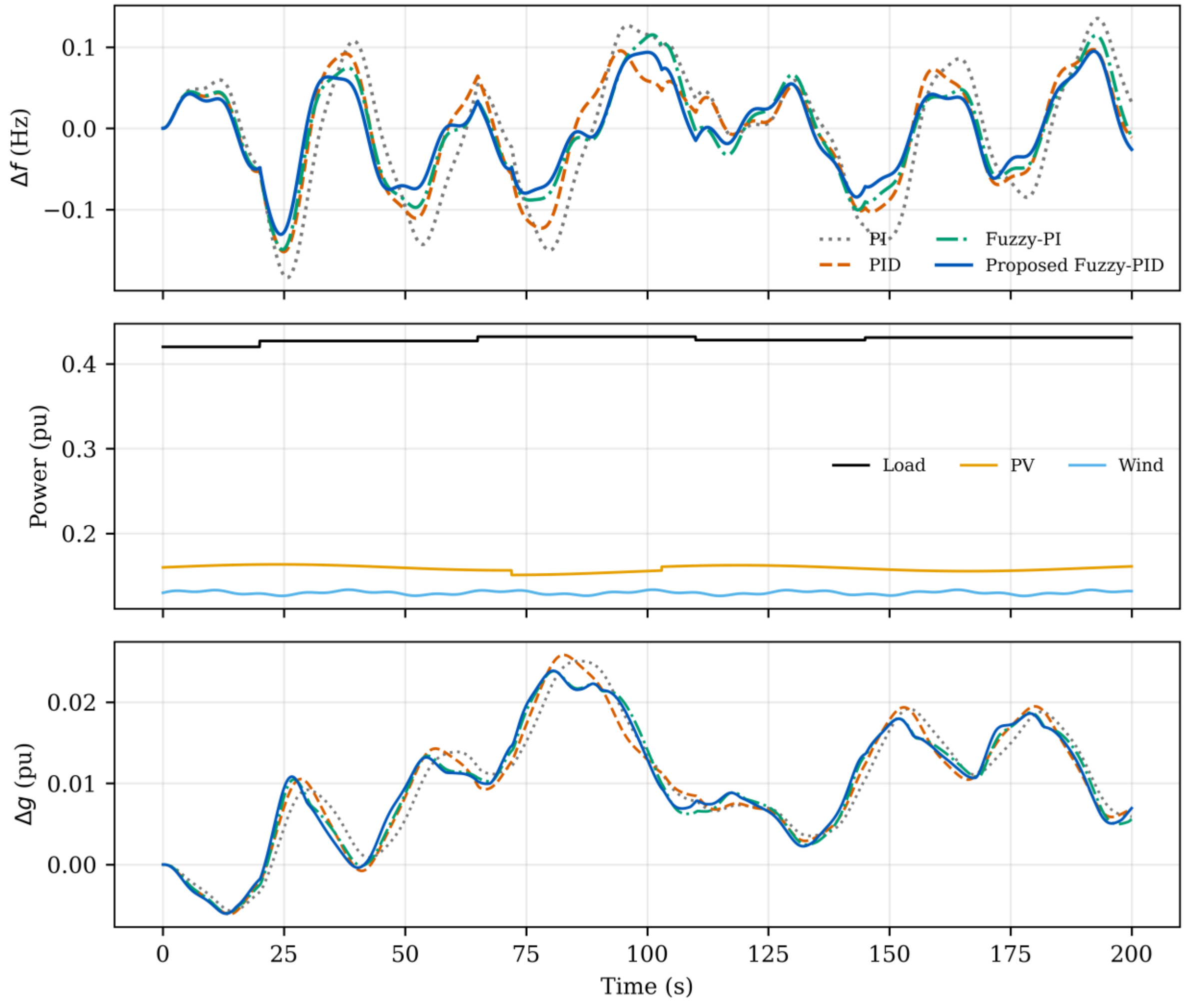

Fig. 3. Scenario 1: frequency, power profiles, and gate responses under mixed load and renewable variations.

As shown in Fig. 3, the fixed PI loop remains stable but leaves visibly broader excursions after each power change. PID adds damping. Fuzzy-PI improves the mid-frequency response, yet it cannot reshape derivative action. Fuzzy-PID therefore separates most clearly after the PV ramp and the final load step. Its peak deviation is 0.1307 Hz; the corresponding values are 0.1840 Hz for PI, 0.1521 Hz for PID, and 0.1493 Hz for fuzzy-PI.

Table 3. Scenario 1 performance indices.

Controller	Peak (Hz)	RMS (Hz)	IAE	ISE	ITAE	ITSE
PI	0.1840	0.0803	13.345	1.289	1334.43	124.91
PID	0.1521	0.0644	10.888	0.829	1054.68	75.91
Fuzzy-PI	0.1493	0.0603	9.984	0.727	988.33	69.59
Fuzzy-PID	0.1307	0.0518	8.630	0.536	846.65	50.29

The proposed controller reduces IAE by 35.3% relative to PI, 20.7% relative to PID, and 13.6% relative to fuzzy-PI. The ISE reduction relative to fixed PID is 35.3%. ITSE falls by 33.8%. These two squared-error results are important: the improvement is not created by redistributing one large excursion into many smaller ones.

B. Severe combined disturbance

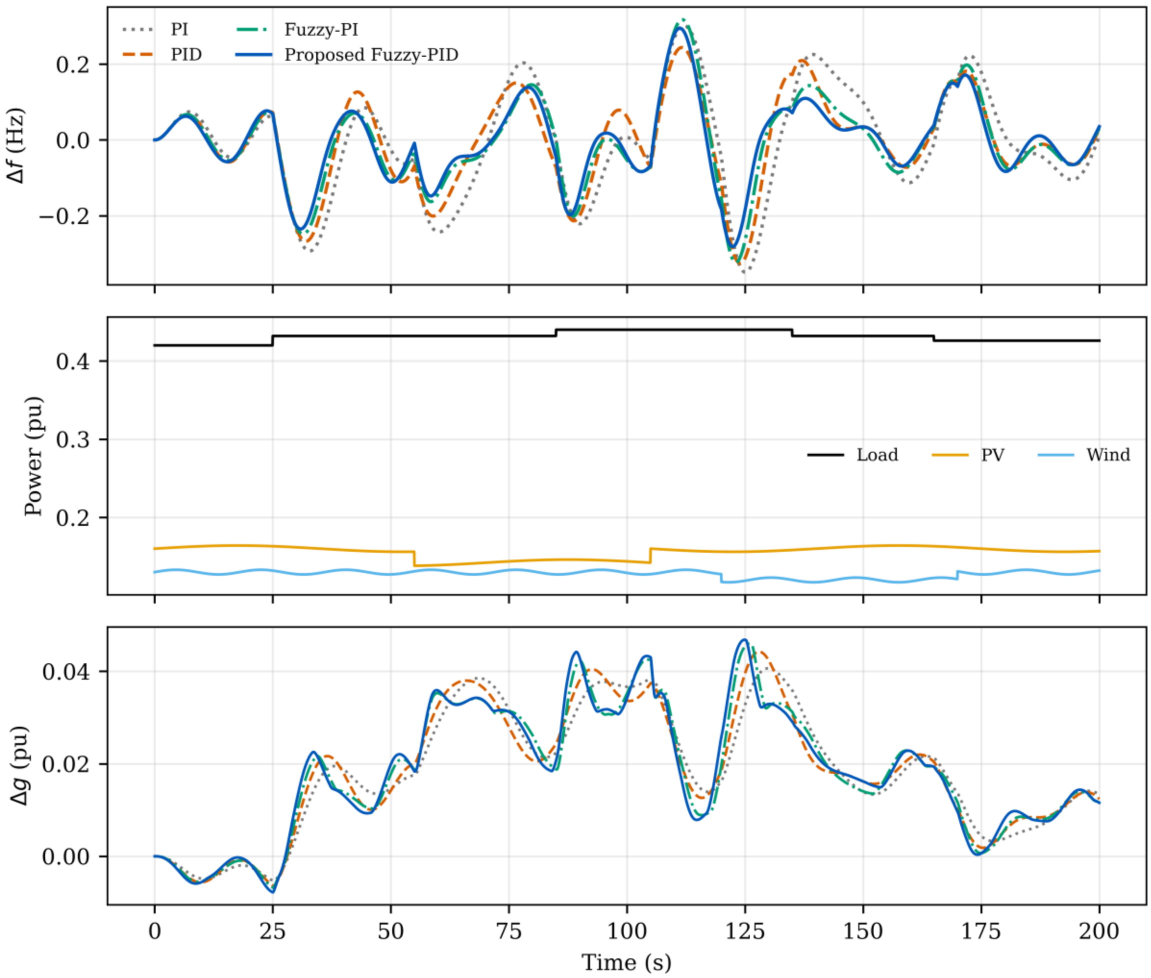

Fig. 4. Scenario 2: response to a large load increase, prolonged PV deficit, load pulse, and wind-power reduction.

Figure 4 tests a less forgiving sequence. The PV loss arrives before the temporary load pulse has fully developed; the subsequent wind deficit prolongs the imbalance. All four controllers remain bounded. Still, the differences widen. Fuzzy-PID limits the peak deviation to 0.2946 Hz, whereas PI reaches 0.3488 Hz. Its IAE is 15.407 Hz·s, 17.9% below PID and 11.5% below fuzzy-PI. The RMS gate commands remain close: 0.02261-0.02280 pu. Thus, the lower frequency error is not purchased by a material increase in gate travel.

Table 4. Scenario 2 performance indices.

Controller	Peak (Hz)	RMS (Hz)	IAE	ISE	ITAE	ITSE
PI	0.3488	0.1430	22.693	4.092	2335.50	416.66
PID	0.3253	0.1195	18.775	2.858	1837.86	278.69
Fuzzy-PI	0.3230	0.1136	17.412	2.580	1770.16	265.41
Fuzzy-PID	0.2946	0.1015	15.407	2.059	1525.16	204.90

C. Persistent multisine disturbance

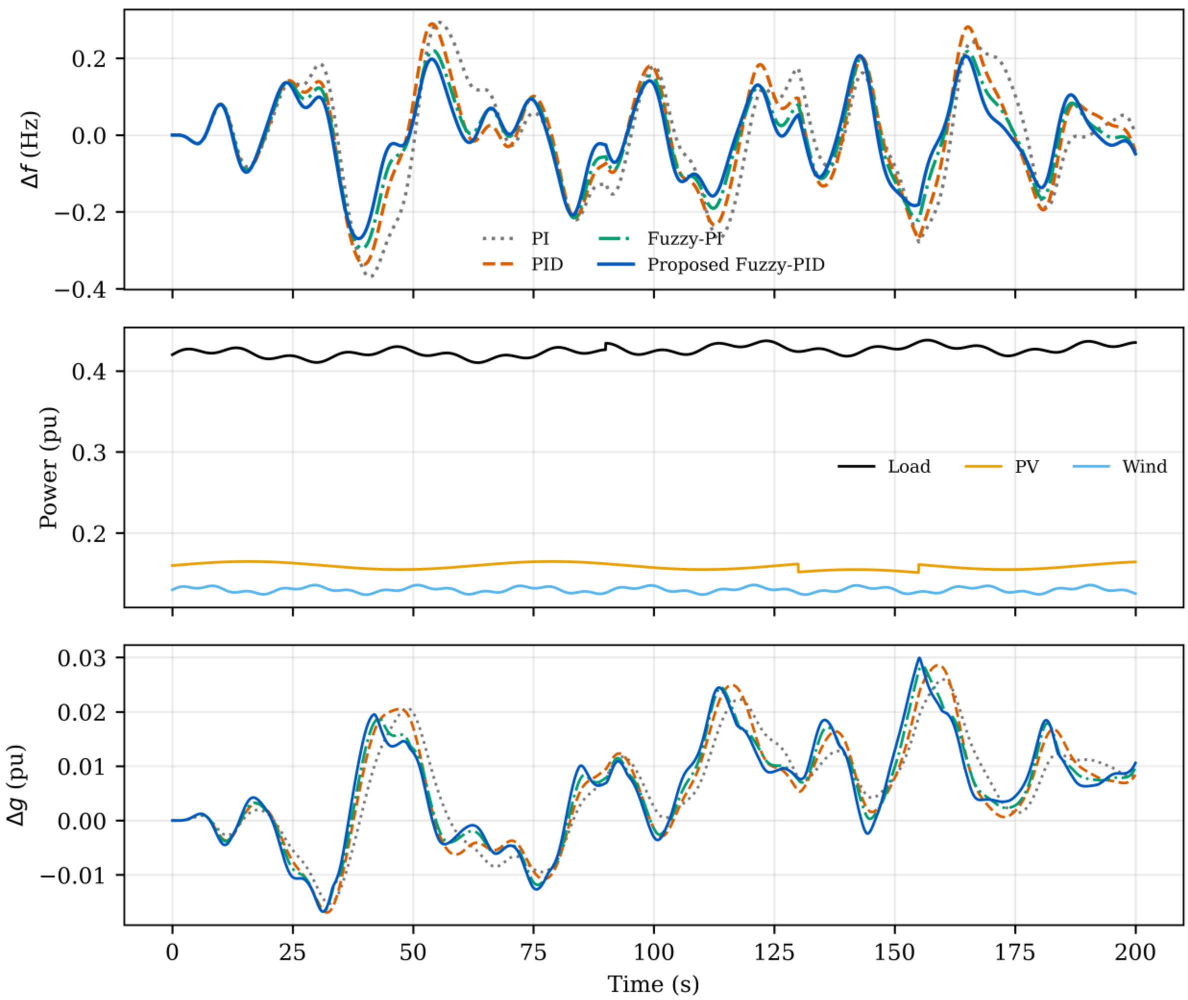

Fig. 5. Scenario 3: persistent multisine load/renewable variations with a short PV cloud event.

The pattern in Fig. 5 is different. There is no long interval in which the loop can settle. Fixed PID lowers the peak relative to PI, but its error energy remains high. Fuzzy-PID gives the smallest peak (0.2696 Hz), IAE (16.146 Hz·s), ISE (2.061 $Hz^2 \cdot s$), ITAE (1608.71 $Hz \cdot s^2$), and ITSE (199.31 $Hz^2 \cdot s^2$). This consistency across absolute and squared criteria is stronger evidence than a single settling-time comparison.

D. Parametric robustness

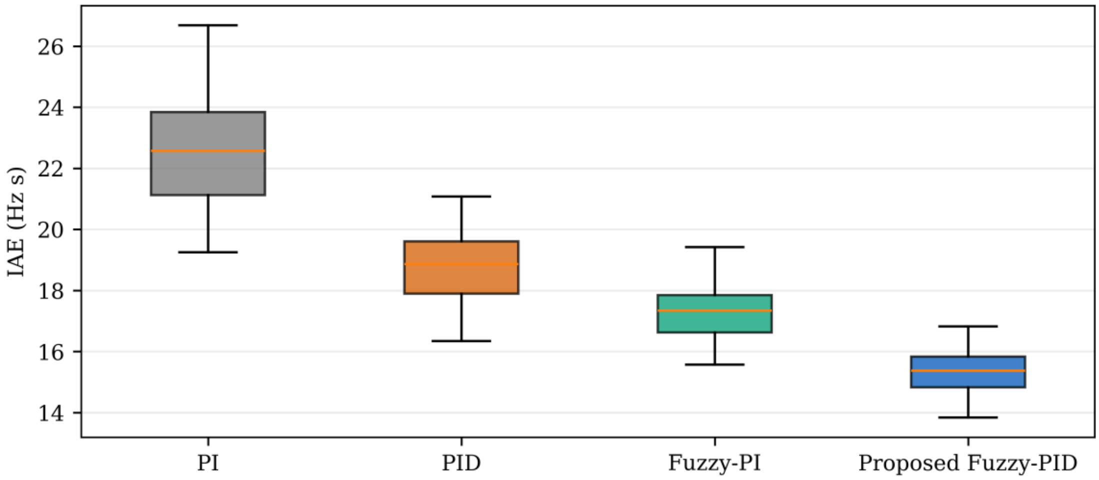

Fig. 6. Forty-run IAE distributions for Scenario 2 under independent ±20% variations of H, D, Tg, and Tw.

Figure 6 preserves the same ordering across forty uncertain plants. Median IAE values are 22.574, 18.866, 17.336, and 15.369 Hz·s. The worst fuzzy-PID realization reaches 17.605 Hz·s, still below the median fixed-PID value. No unstable run is observed. This is an empirical robustness evidence.

E. Interpretation, limitations, and implementation

The proposed scheduler combines three useful behaviors: fast proportional reinforcement, derivative damping during rapid power imbalance, and restrained integral accumulation. Comparable benefits of fuzzy, predictive, and renewable-aware frequency control have been reported in [9]-[15]. Detailed PV dynamics are treated in [16], while PV-plus-storage frequency support is studied in [17]. Autonomous multi-agent coordination is developed in [18], and high-wind islanded operation is examined in [19]. Pumped-hydro and battery participation are considered in [20]. Fractional and soft-computing developments are reviewed in [21], [22]. Those studies support the modelling choices, but they do not substitute for the controlled four-controller comparison performed here.

The evidence remains simulation based. The hydraulic model excludes elastic water hammer, head-dependent efficiency, backlash, and penstock resonance. Converter current limits, measurement noise, protection logic, and communication delay are also omitted. Practical implementation should add bumpless gain transfer, a derivative filter, supervisory fallback gains, and a gate-duty monitor. Hardware-in-the-loop testing is therefore the next defensible step—not an optional embellishment.

VI. CONCLUSION

An interpretable fuzzy-PID governor has been evaluated for an isolated hydro-PV-wind grid. The assessment used three disturbance scenarios, four integral criteria, common actuator limits, and forty independently perturbed plants. Fuzzy-PID achieved the lowest peak, RMS, IAE, ISE, ITAE, and ITSE values in every deterministic scenario. Under the severe test, its IAE was 15.407 Hz·s, compared with 18.775 Hz·s for fixed PID and 17.412 Hz·s for fuzzy-PI. The uncertainty study retained that ranking. These results support the value of simultaneous proportional, integral, and derivative scheduling; they do not yet establish field readiness. Higher-order hydraulic modelling and hardware-in-the-loop validation remain necessary.

REFERENCES

[1] H. H. Alhelou, M. E. H. Golshan, R. Zamani, E. Heydarian-Forushani, and P. Siano, "Challenges and opportunities of load frequency control in conventional, modern and future smart power systems: A comprehensive review," Energies, vol. 11, no. 10, 2497, 2018. doi: 10.3390/en11102497.

[2] K. Ullah, A. Basit, Z. Ullah, S. Aslam, and H. Herodotou, "Automatic generation control strategies in conventional and modern power systems: A comprehensive overview," Energies, vol. 14, no. 9, 2376, 2021. doi: 10.3390/en14092376.

[3] M. Ranjan and R. Shankar, "A literature survey on load frequency control considering renewable energy integration in power system: Recent trends and future prospects," Journal of Energy Storage, vol. 45, 103717, 2022. doi: 10.1016/j.est.2021.103717.

[4] R. Asghar et al., "A review of load frequency control schemes deployed for wind-integrated power systems," Sustainability, vol. 15, no. 10, 8380, 2023. doi: 10.3390/su15108380.

[5] D. H. Tungadio and Y. Sun, "Load frequency controllers considering renewable energy integration in power system," Energy Reports, vol. 5, pp. 436-453, 2019. doi: 10.1016/j.egyr.2019.04.003.

[6] W. Guo and J. Yang, “Modeling and dynamic response control for primary frequency regulation of hydro-turbine governing system with surge tank,” Renewable Energy, vol. 121, pp. 173-187, 2018. doi: 10.1016/j.renene.2018.01.022.
[7] T. Reigstad and K. Uhlen, “Variable-speed hydropower generation: System modeling, optimal control, and experimental validation,” IEEE Transactions on Industrial Electronics, vol. 68, no. 11, pp. 10902-10912, 2021. doi: 10.1109/TIE.2020.3031528.
[8] U.S. Department of Energy, Hydropower Modeling Gaps in Planning and Operational Studies, 2022. URL: https://www.energy.gov/sites/default/files/2023-07/HydropowerModelingGaps.pdf.
[9] Y. Arya, “Automatic generation control of two-area electrical power systems via optimal fuzzy classical controller,” Journal of the Franklin Institute, vol. 355, pp. 2662-2688, 2018. doi: 10.1016/j.jfranklin.2018.02.004.
[10] S. Kayalvizhi and D. M. V. Kumar, “Load frequency control of an isolated micro grid using fuzzy adaptive model predictive control,” IEEE Access, vol. 5, pp. 16241-16251, 2017. doi: 10.1109/ACCESS.2017.2735545.
[11] N. Jalali, H. Razmi, and H. Doagou-Mojarrad, “Optimized fuzzy self-tuning PID controller design based on Tribe-DE optimization and rule-weight adjustment for load frequency control of interconnected multi-area power systems,” Applied Soft Computing, vol. 93, 106424, 2020. doi: 10.1016/j.asoc.2020.106424.
[12] A. H. Yakout, H. Kotb, H. M. Hasanien, and K. M. AboRas, “Optimal fuzzy PIDF load frequency controller for hybrid microgrid system using marine predator algorithm,” IEEE Access, vol. 9, pp. 54220-54232, 2021. doi: 10.1109/ACCESS.2021.3070076.
[13] A. H. Yakout, H. M. Hasanien, and A. Al-Durra, “A novel ultra-local based-fuzzy PIDF controller for frequency regulation of hybrid microgrids,” Processes, vol. 11, no. 4, 1093, 2023. doi: 10.3390/pr11041093.
[14] P. C. Sahu et al., “A robust DQN based grade-2 fuzzy cascaded controller for load frequency control of islanded microgrid,” e-Prime - Advances in Electrical Engineering, Electronics and Energy, vol. 6, 100288, 2023. doi: 10.1016/j.prime.2023.100288.
[15] İ. Türk and H. Gözde, “Robust load frequency control in hybrid microgrids using type-3 fuzzy logic,” Symmetry, vol. 17, no. 6, 853, 2025. doi: 10.3390/sym17060853.
[16] A. Bakeer, G. Magdy, A. Chub, and H. Bevrani, “A sophisticated modeling approach for photovoltaic systems in load frequency control,” International Journal of Electrical Power & Energy Systems, vol. 134, 107330, 2022. doi: 10.1016/j.ijepes.2021.107330.
[17] L. Liu et al., “Load frequency control for renewable energy sources for isolated power system by introducing large scale PV and storage battery,” Energy Reports, vol. 6, pp. 1597-1603, 2020. doi: 10.1016/j.egyr.2020.12.030.
[18] D. Yu, H. Zhu, W. Han, and D. Holburn, “Dynamic multi agent-based management and load frequency control of PV/fuel cell/wind turbine/CHP in autonomous microgrid system,” Energy, vol. 173, pp. 554-568, 2019. doi: 10.1016/j.energy.2019.02.094.
[19] R. KazemiGolkhandan, H. Torkaman, M. R. Aghaebrahimi, and A. Keyhani, “Load frequency control of smart isolated power grids with high wind farm penetrations,” IET Renewable Power Generation, vol. 14, no. 7, pp. 1228-1238, 2020. doi: 10.1049/iet-rpg.2019.0601.
[20] H. H. Coban, A. F. Zobaa, and B. Ç. Erdinç, “Load frequency control of microgrid system by battery and pumped-hydro energy storage,” Water, vol. 14, no. 11, 1818, 2022. doi: 10.3390/w14111818.
[21] P. Wang et al., “Fractional-order load frequency control of an interconnected power system considering renewable-energy randomness,” Fractal and Fractional, vol. 8, no. 3, 126, 2024. doi: 10.3390/fractalfract8030126.
[22] B. Singh et al., “Review on soft-computing-based controllers for frequency regulation of renewable-rich power systems,” Energies, vol. 16, no. 4, 1917, 2023. doi: 10.3390/en16041917.